POLITECNICO DI TORINO
Repository ISTITUZIONALE

Quantum Readout of Imperfect Classical Data

Original
Quantum Readout of Imperfect Classical Data / Ortolano, G., Ruo-Berchera, I.. - In: SENSORS. - ISSN 1424-8220. - ELETTRONICO. - 22:6(2022), p. 2266. [10.3390/s22062266]

Availability:
This version is available at: 11583/2972751 since: 2022-11-02T16:30:04Z

Publisher:
MDPI

Published
DOI:10.3390/s22062266

Terms of use:

This article is made available under terms and conditions as specified in the corresponding bibliographic description in the repository

Publisher copyright

(Article begins on next page)

29 November 2026

sensors

MDPI

Article

Quantum Readout of Imperfect Classical Data

Giuseppe Ortolano [1,2] and Ivano Ruo-Berchera [1,*]

[1] Istituto Nazionale di Ricerca Metrologica, Strada Delle Cacce, 10135 Torino, Italy; giuseppe.ortolano@polito.it
[2] Department of Applied Science and Technology, Politecnico di Torino, Corso Duca degli Abruzzi 24, 10129 Torino, Italy
* Correspondence: i.ruoberchera@inrim.it

Abstract: The encoding of classical data in a physical support can be done up to some level of accuracy due to errors and the imperfection of the writing process. Moreover, some degradation of the stored data can happen over time because of physical or chemical instability of the system. Any readout strategy should take into account this natural degree of uncertainty and minimize its effect. An example are optical digital memories, where the information is encoded in two values of reflectance of a collection of cells. Quantum reading using entanglement, has been shown to enhances the readout of an ideal optical memory, where the two level are perfectly characterized. In this work, we analyse the case of imperfect construction of the memory and propose an optimized quantum sensing protocol to maximize the readout accuracy in presence of imprecise writing. The proposed strategy is feasible with current technology and is relatively robust to detection and optical losses. Beside optical memories, this work have implications for identification of pattern in biological system, in spectrophotometry, and whenever the information can be extracted from a transmission/reflection optical measurement.

Keywords: quantum channel discrimination; quantum hypothesis testing; quantum enhanced measurement

check for updates

Citation: Ortolano, G.; Ruo-Berchera, I. Quantum Readout of Imperfect Classical Data. *Sensors* **2022**, *22*, 2266. https://doi.org/10.3390/s22062266

Academic Editor: Ming-Jie Sun

Received: 1 February 2022
Accepted: 11 March 2022
Published: 15 March 2022

Publisher's Note: MDPI stays neutral with regard to jurisdictional claims in published maps and institutional affiliations.

Copyright: © 2022 by the authors. Licensee MDPI, Basel, Switzerland. This article is an open access article distributed under the terms and conditions of the Creative Commons Attribution (CC BY) license (https://creativecommons.org/licenses/by/4.0/).

1. Introduction

The use of quantum resources, such as quantum correlations and squeezing, has allowed to surpass classically imposed limits on a variety of practical tasks. Restricting to the optical domain, quantum metrology and sensing [1–3] shows the possibility to improve parameter estimation [4], such as phase [5–7] and transmission [8–10], with relevant applications both to technology [11,12] and fundamental physics [13–15]. In quantum hypothesis testing [16,17], a certain number of protocols have been proposed, in particular the quantum illumination [18–22] addressed to target detection in a noisy background and the quantum reading (QR) [23–29] , capable of improving the readout of data stored in classical digital memories. In classical memories information is encoded in a physical object for later reuse, and a successful readout also depends on the reliability of the writing (encoding) process. An example are optical digital memories, where the information is encoded in two possible values of the reflectance (or equivalently transmittance) of a collection of cells. In this context, the QR protocol [23] shows a significant quantum enhancement of the readout performance, in terms of bits extracted from a cell for a fixed energy. Single cell QR has been recently realized experimentally [30] and has been theoretically generalized to a more realistic multicell scenario [31–34]. While those limits are important in gauging the possible improvement offered by quantum resources over classical strategies, in a more application oriented approach, it is useful to consider the case in which the transmittance values cannot be reproduced with arbitrary precision, rather they can be more realistically represented by classical random variables whose distributions can be eventually characterized. The scenario could be the one of a commercial production, with a limited single-cell accuracy, but with the possibility of an extremely precise post-

production characterization. This problem studied here has some analogy to the recently proposed task of Quantum Conformance Test (QCT) [35], although the goal is different, the last one being devoted to the recognition of a defective production process with respect to a standard. In this work, we analyse the effect of possible defects in the construction of the memory on the readout performance and maximize the readout accuracy in presence of an imperfect, yet characterized, writing process.

Moreover, we extend the analysis of QR with imperfect cells by considering a more general classical benchmark that takes into account a multicell memory and a collective measurement of the probed cells, showing that cell-by cell quantum readout remains anyway better in recovering the stored information. A multicell memory can be seen as a large block of cells for which the information is stored, according to some classical encoding, in classical codewords expressed by cells (quantum channels). In the limit of very large memories (infinte number of cells) the maximum amount of information retrieved can by found with a constrained (at fixed energy) optimization of the Holevo bound [36–38], that we solve in the case of classical input states and imperfect encoding.

2. Materials and Methods

2.1. Optical Memory and Readout Model

Let us consider an optical memory composed by D cells, each storing one bit of information in two possible values of trasmittance τ_0 and τ_1. The readout of each cell is carried out using a transmitter emitting a bipartite optical probe in a state ρ. Let us call the two systems of the bipartite state signal (S) and idler (I) system. A number M of optical modes in the signal system are sent to the cell while L modes of the idler system are sent directly to a receiver where a general joint POVM with the returning signal is performed. A decision on the value, $y = 0, 1$, of the stored bit is taken after classical post processing of the measurement result. A schematic of the protocol is given in Figure 1A. The optical transmittance acting on the signal modes can be modelled by means of a pure loss quantum channel $\mathcal{E}_\tau$, so that the state at the receiver can be written as $\sigma_\tau = (\mathcal{E}_\tau \otimes \mathcal{I})\rho$, where $\mathcal{I}$ is the identity operator acting on the idler modes. The problem of information recovery can then be seen as a problem of quantum channel discrimination [39,40] between two channels, $\mathcal{E}_{\tau_0}$ and $\mathcal{E}_{\tau_1}$, with the minimum probability of error. When the discrimination is performed using optical states that live in an infinite dimensional Hilbert space, a non trivial formulation of the problem requires that some constraint are imposed on the input states [41]. A common choice, that we adopt here, is to fix the energy of the signal system. The constrained minimization of the probability of error is a double optimization problem, both on the input state ρ and on the measurement performed at the receiver. In case of a perfectly characterized memory, for which τ_0 and τ_1 are known with arbitrary accuracy, ultimate theoretical limits on the readout performance have been found [23,24,31].

A single cell of an imperfect optical memory stores one bit of information in one of two possible random values of transmittance, T_i, with $i = 0, 1$, each with a probability distribution $g_i(\tau_i)$. The problem of information retrieval from an imperfect memory cell remains formally similar to the perfect memory one, namely it remains a quantum channel discrimination problem, but the channel to be discriminated are convex combinations of pure loss channels $\mathcal{E}_\tau$. In particular a bipartite input state ρ irradiated by the transmitter will be mapped to the state ρ_i:

$$\rho_i = \mathbb{E}_{g_i}[(\mathcal{E}_{\tau_i} \otimes \mathcal{I})\rho] \tag{1}$$

where $i = 0, 1$ and $\mathbb{E}_{g_i}[\cdot]$ denotes the expectation value over the distribution g_i. The problem of discriminating two channels in the form defined by Equation (1) has been analysed in a different context in the QCT protocol [35]. Bipartite classical states are defined as the class of convex combinations of coherent states:

$$\rho^{cla} = \int d^{2M}\boldsymbol{\alpha}\, d^{2L}\boldsymbol{\beta}\, P(\boldsymbol{\alpha}, \boldsymbol{\beta}) |\boldsymbol{\alpha}\rangle\langle\boldsymbol{\alpha}| \otimes |\boldsymbol{\beta}\rangle\langle\boldsymbol{\beta}| \tag{2}$$

where $|\boldsymbol{\alpha}\rangle = |\alpha_1, \ldots, \alpha_M\rangle$ and $|\boldsymbol{\beta}\rangle = |\beta_1, \ldots, \beta_L\rangle$ are M and L mode coherent states for signal and idler respectively. In Ref. [35] it was shown how fixing the mean number of signal

photons μ, that in terms of Equation (2) defines the constraint $\int d^{2M}\boldsymbol{\alpha}\, d^{2L}\boldsymbol{\beta}\, P(\boldsymbol{\alpha},\boldsymbol{\beta})|\boldsymbol{\alpha}|^2 = \mu$, classical states have a probability of error in the discrimination, for a cell prepared with equal probability in T_0 or T_1, namely $p_0 = p_1 = 1/2$, that is lower bounded by:

$$p_{err}^{cla} \geq \frac{1 - \mathbb{E}_{g_0}\left[\mathbb{E}_{g_1}\left[\sqrt{1 - e^{-\mu\left(\sqrt{\tau_0}-\sqrt{\tau_1}\right)^2}}\right]\right]}{2} \tag{3}$$

for any output measurement. This limit can be derived starting by the optimal probability of error in discriminating the states ρ_0 and ρ_1 given by the Helstrom bound [16] $p_{err}^{HB} = (1 - D(\rho_0, \rho_1))/2$, where $D(\rho_0, \rho_1)$ is the trace distance, and using the convexity of $D(\rho_0, \rho_1)$ to lower bound the probability of error. The use non classical states, in particular two mode squeezed vacuum states [42,43] paired with photon counting measurements allows to surpass the classical limit in Equation (3).

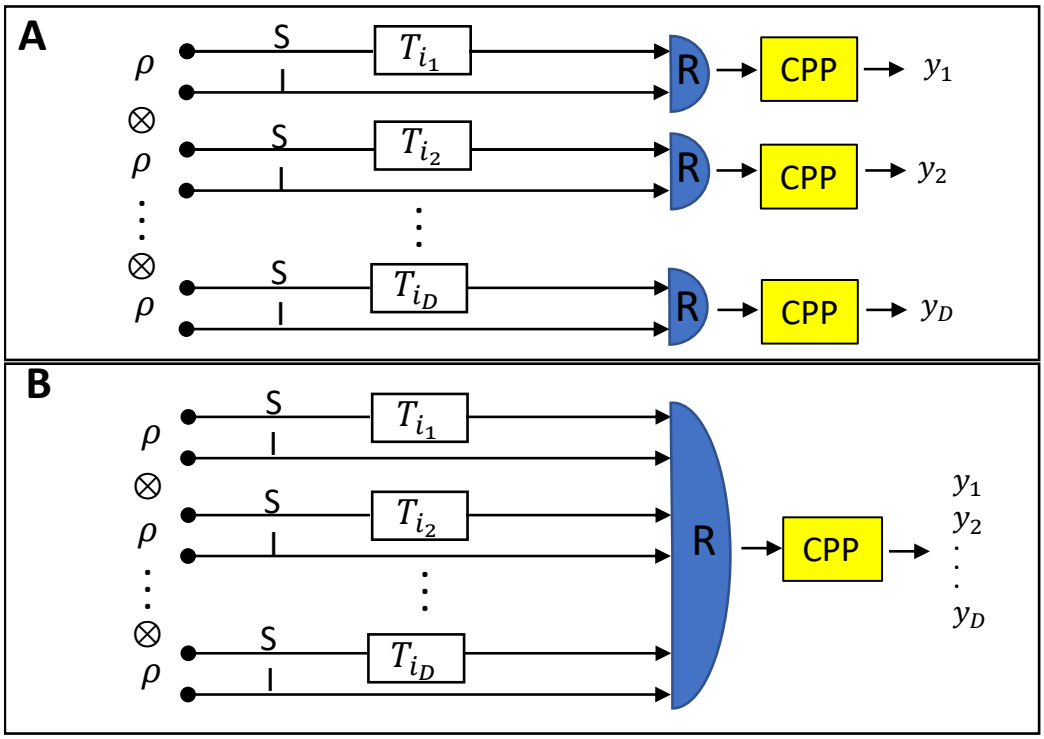

Figure 1. Memory readout scheme. (**A**) *Local readout.* A memory is depicted by an array of D cells, each represented by the transmittance T_i, $i = 0, 1$. T_i is in general a random variable, but in the case of a perfect cell it reduces to a single parameter τ_i. A bipartite state ρ is irradiated by a transmitter. The signal (S) system interacts with the memory cell while the idler (I) is sent directly to a local receiver (R) where it is measured jointly with the signal. The value of the bit is determined by classical post-processing (CPP) of the measurement result. (**B**) *Global readout.* If an array of length D (a memory) is tested in parallel, instead of cell by cell, D copies of ρ are sent to the cells, one for each, and a joint measurement between all the copies is performed.

In the context of memory reading, a more fitting figure of merit is the information recovered by the procedure. We consider once again and from here on after cells prepared with equal probability, $p_0 = p_1 = 1/2$. Given the probability of error p_{err} the information recovered I is:

$$I = 1 - H(p_{err}) \tag{4}$$

where $H(p) = -p\log_2 p - (1-p)\log_2(1-p)$ is the binary Shannon entropy. In the following, we will compare the performance of a specific local quantum read-out strategy, where local means that each cell is probed and measured separately, with respect to three

different classical benchmarks: The local optimal one, the local based on a specific receiver (photon counting), and finally a global optimal one. In the last one, an array of D cells is probed by a tensor product state $\rho^{\otimes D}$, and the receiver is allowed to perform a collective measurement across the memory, as it is depicted in Figure 1B.

2.2. Local Classical Limits

Consider the scheme in Figure 1A, and a classical input state as defined in Equation (2). In a local configuration each cell is probed independently and the probability of error is lower bounded by the expression in Equation (3), meaning that the information recovered will be upper bounded by:

$$\mathcal{C}^{HB} := 1 - H(p_{err}^{cla}) \tag{5}$$

where we chose the superscript HB to denote this limit since the derivation of p_{err}^{cla} is based on the Helstrom bound, as mentioned before.

The limit in Equation (5) refers to an optimal unspecified detection scheme. Because of a certain number of inequality used to recover it, this lower bound is expected to be not tight, meaning that it could not be reachable. Moreover, the measurement scheme required to achieve an optimal performance could involve complex operations difficult to implement practically. For those reasons, it is useful to consider a second local classical benchmark, fixing a specific receiver. In particular, we will consider a receiver consisting of photon counting measurements, followed by a maximum likelihood post-processing decision. When considering photon counting measurements the characterizing quantity is the conditional photon number distribution at the receiver, $p(\mathbf{n}|T_i) = \langle \mathbf{n}|\rho_i|\mathbf{n}\rangle$, where $\mathbf{n} = (n_S, n_I)$ is the number of measured photons in the idler and signal systems. After the measurement the optimal choice to recover the value of the bit y is to choose it as $y = \arg\max_i p(T_i|\mathbf{n})$, a condition that, using Bayes theorem and the fact that we assumed $p_0 = p_1 = 1/2$, is equivalent to $y = \arg\max_i p(\mathbf{n}|T_i)$, i.e., to maximize the likelihood. In terms of photon number distribution the probability of error of the recovery with a photon counting receiver, p_{err}^{PC}, is given by [35]:

$$p_{err}^{PC} = \frac{1}{2}\sum_{\mathbf{n}} \min_i p(\mathbf{n}|T_i) \tag{6}$$

i.e., the probability of error is proportional to the overlap of the measurement outcome distributions $p(\mathbf{n}|T_0)$ and $p(\mathbf{n}|T_1)$. For classical states the outcome distribution overlap cannot be reduced using idler modes, that are therefore not needed in this setting, and the overlap will be minimized for input signal states having a Poisson distribution in the photon number, such as a single mode coherent state [35]. Computing the probability of error in Equation (6) for a Poisson distributed input signal state, that we denote as $p_{err}^{cla,PC}$, we can define a second informational limit:

$$\mathcal{C}^{PC} := 1 - H(p_{err}^{cla,PC}) \tag{7}$$

The limit $\mathcal{C}^{PC}$ defines the maximum information recovered per cell for a local strategy using classical states and photon counting measurements. Under certain assumptions $p_{err}^{cla,PC}$ can be written in a closed form, otherwise it can be computed numerically, a detailed discussion on the computation of this probability of error is given in Ref. [35].

2.3. Local Quantum Strategy

Let us consider now input states not belonging to the class defined by Equation (2), i.e., non-classical states. In particular we choose a collection $\rho = \bigotimes^M |TMSV\rangle_{I,S}$, of M Two Mode Squeezed Vacuum (TMSV) states, represented in the Fock base $\{|n\rangle\}$ as:

$$|TMSV\rangle_{I,S} \propto \sum_n \sqrt{P_\mu(n)}|n\rangle_P|n\rangle_R, \tag{8}$$

where $P_\mu(n) = \mu^n/(\mu+1)^{n+1}$ is a thermal distribution with mean photon μ. It is a bipartite maximally entangled state with perfectly correlated number of photons of the signal and idler systems [44–46]. We have in this case $L = M$. After the interaction with the memory cell the receiver performs a photon counting measurement, both at the signal and idler systems, with outcome $\mathbf{n} = (n_S, n_I)$. Then, a value y is assigned to the recovered bit, according to the procedure described in the previous section for the photon counting receiver, as $y = \arg\max_i p(\mathbf{n}|T_i)$. In this case the quantum correlated idler results in a reduction of the overlap of the outcome distribution, a purely quantum feature that cannot be reproduced with classical states.

The steps for the derivation of the probability of error, $p_{err}^{qua,PC}$, can be found in [35], and we do not report them here. Although an analytical compact expression for the error probability cannot be achieved, a numerical analysis is possible. We denote the information recovered using the quantum strategy as:

$$\mathcal{Q} := 1 - H(p_{err}^{qua,PC}). \tag{9}$$

2.4. Global Classical Limit

A memory is constituted by an array of D cells. In terms of information, the single cell can be seen as encoding the binary r.v. X in the ensemble $\{p_i, \rho_i\}$, $i = 0, 1$. If the array of lenght D can be probed in parallel and a joint measurement on all the output is allowed, a direct encoding (one bit per cell) may not be the more efficient storing strategy. In general, the information will be encoded in codewords onto the array of cells. For the retrieval, in the following we will consider strategies in which each cell is probed by a copy of a state ρ, so that the total probing state is of the form $\rho^{\otimes D}$. The information is then recovered by a joint global POVM measurement at the output (see Figure 1B). The multicell storage/retrieval of information is a transfer of information through the memory, characterized in terms of quantum channels, and the maximum rate of information I^D that can be retrieved per single channel use (cell of the memory) is upper bounded [31] by the Holevo quantity χ:

$$I^D \leq \chi(\rho) := S(\rho) - \sum_i p_i S(\rho_i) \tag{10}$$

where $\rho = \sum_i p_i \rho_i$ and $S(\rho) = -\mathrm{Tr}(\rho \log \rho)$ is the von-Neumann entropy [47]. In this case $i = 0, 1$, ρ_i are the states defined in Equation (1) and p_i is the probability for the cell to be prepared with either one of the values of T_i. In case of $D \to \infty$, that could be the case for very large memories, the Holevo-Schumacher-Westmoreland (HSW) theorem [47] will assure that it exist a POVM such that the information will converge to χ. Computing the bound in Equation (10) is a difficult task. The maximization becomes significantly easier if we restrict to the class of classical input states defined by Equation (2). We can then define the maximum global classical information, χ_{cla}, as the maximization of χ over all classical states:

$$\chi_{cla} := \max_{\rho_{cla}} \chi(\rho) \tag{11}$$

Details on how the calculation of this limit is performed are reported in Appendix A.

Of course one can expect that a global quantum strategy, where the quantum probe is paired with a global (collective) receiver would perform better than the proposed local quantum strategy. However, the optimization of the Holevo bound is not an easy task for a general quantum state, as mentioned before, and it goes beyond the scope of this work, which is to demonstrate that there exists at least a quantum strategy beating the global classical bound.

3. Results

To compare the quantum strategy with the three classical ones presented in the previous section we assume that the distributions $g_i(\tau_i)$ of the random variable T_i are Gaussian and we denote the mean value as $\bar{\tau}_i$ and the standard deviation as σ_i. In Figure 2 we report the results, in terms of information recovered per cell, for two possible configurations of

the transmittance's distributions. The first row shows a case in which the overlap between g_0 and g_1 is negligible. This means that, although the transmittance values are uncertain, in principle the value of the bit is codified in an unambiguous way, and a perfect measurement would be able to discriminate correctly its value. However, quantum fluctuations introduce further noise which reduce the actual distinguishability. In panel A, we show the information recovered as a function of the mean number of signal photons μ. The information recovered increases as the signal energy is increased, up until it saturates at the maximum amount of information for a single binary cell, i.e., 1 bit. In the range showed this saturation is only visible for the local quantum strategy, $\mathcal{Q}$ (reported in red), that reaches it earlier than any of the classical one, even earlier than the global capacity bound χ. It shows that the use of quantum resources allows a reliable recovery of the information with significantly less energy than otherwise needed. In Panel B, we fix the number of photons but let $\bar{\tau}_0$ vary, while keeping fixed all the other parameter of the distributions. As expected, the recovered information is higher when $\bar{\tau}_0$ is far from the fixed mean value $\bar{\tau}_1$ and starts to decrease when the two values get too close. However, in the quantum case, the strong degree of correlation of the source can be used to reduces the quantum fluctuations, which reflects in a much narrower low-informative region, the deep in Figure 2B. The second row of Figure 2, presents the case of a relevant overlapping of the initial distributions, obtained by increasing their standard deviations, as reported in the bottom-left box. In panel C and D, we show the dependence on the mean photon number μ and the transmittance $\bar{\tau}_0$. Note that the information saturates at a value smaller than 1 bit (specifically 0.8) because the initial overlapping of the distributions. Of course, even a perfect measurement could not unravel the initial ambiguous encoding. In panel D, we see an effect similar to panel B, where the information recovered drops as $\bar{\tau}_0$ approaches the fixed value of $\bar{\tau}_1$. There is, however, a widening of the low-informative region w.r.t the case of non-overlapping distributions. The quantum strategy present still a significant improvement in this scenario were there is a greater part of indistinguishability not due to fluctuations.

We turn now our attention to the quantum gain defined as the difference:

$$G = \mathcal{Q} - \mathcal{C} \tag{12}$$

where $\mathcal{C}$, can represent each one of the three classical bounds defined in Equations (5), (7) and (10), in particular G^{PC}, G^{HB} and G^{χ} is the quantum gain w.r.t $\mathcal{C}^{PC}$, $\mathcal{C}^{HB}$ and χ_{cla} respectively. These quantities are reported in Figure 3 as a contour plot in function of the transmittance $\bar{\tau}_0$ and the number of photons μ, while the other parameters are fixed. In the first row of Figure 3, the standard deviation of both distributions is fixed to $\sigma_0 = \sigma_1 = 0.001$ which are small enough to reduce the initial overlapping. We see how the quantum gain in all three cases is relevant in most of the region analysed. The quantum strategy, based on photon counting measurement, performs very well against the same measurement strategy realized with classical probes, with the gain G^{PC} reaching values above 0.9 bits. Thus, the use of a quantum probe allows recovering almost all the information in a region where the same detection strategy with classical states would fail. A similar result is shown for the gain G^{HB} w.r.t. the optimal local classical bound, although with slightly lower gains, reaching a maximum of 0.8 bits. Even more remarkable it is the gain G^{χ} over the classical global limit, representing the bound on the information recovered per cell after a global measurement, which is significantly higher than zero in a wide region and reaches values higher than 0.7 bits per cell. This shows how the improvement offered by quantum correlation cannot be substituted by any, even not trivial, classical encoding over large memories. In all three panels, the range of transmittance showing a significant advantage is wider for small number of photons, where quantum fluctuations are more relevant. In the second row we show the effect of increasing the standard deviation to $\sigma_0 = \sigma_1 = 0.0025$, leading to a larger overlapping between the initial distributions in the region explored. We see, in general, a reduction of the gain due to the initial ambiguity of the encoding that limit the value of accessible information to a value lower than 1 bit and consequently the space for quantum advantage.

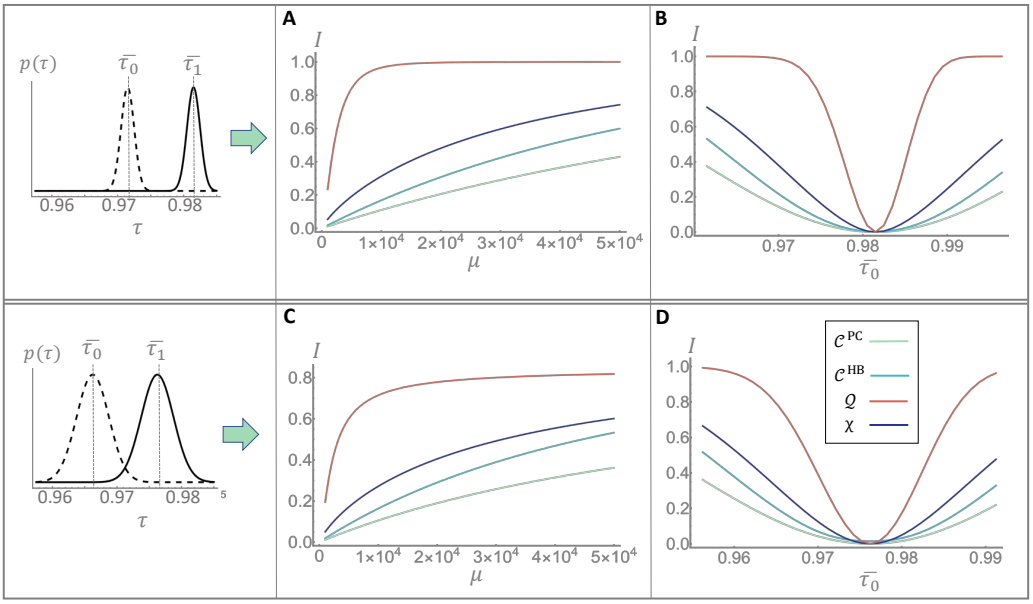

Figure 2. Comparison of information recovery. We compare the information recovered with the three classical strategies and the quantum one, described in the main text, for two different configuration of the trasmittance distributions $g_0(\tau_0)$ and $g_1(\tau_1)$, both assumed gaussian. In the fist row, we fixed the mean value of g_1 to $\bar{\tau}_1 = 0.982$ and the standard deviations of the distributions to $\sigma_1 = \sigma_0 = 0.001$. In panel (**A**), the mean value of g_0 is fixed to $\bar{\tau}_0 = 0.972$ and the informations are showed as a function of the mean number of signal photons μ. In all the panels we report the quantum recovered information $\mathcal{Q}$ in red, the global classical bound χ in dark blue, the local classical bound $\mathcal{C}^{HB}$ in light-blue and the photon counting classical performance in light green. In panel (**B**) we fixed the photon number to $\mu = 10^4$ and we showed the information in function of $\bar{\tau}_0$. In the second row, we set different transmittance distributions, in order to increase their overlap, with (panel (**C**)) $\bar{\tau}_1 = 0.976$, $\bar{\tau}_0 = 0.966$ and $\sigma_1 = \sigma_0 = 0.0025$. In panel (**D**) we fix $\mu = 10^4$ and let $\bar{\tau}_0$ vary.

In experimental realizations, the main issue is the presence of optical losses from various sources. In the present scheme, the photon losses are accounted by the term $1 - \eta$, with the efficiency $0 \leq \eta \leq 1$. For the classical case the losses result simply in an effective reduction of the probing energy from μ to $\eta\mu$. In the quantum case, however, on top of the effective reduction of energy, losses have also an hindering effect on the correlations. The result of taking losses into account is then a reduction of the gain. In Figure 4 we report the the gain for the distribution case of non-overlapping initial distribution for different values of the efficiency. The panel A shows the gain as a function of the number of photons μ. Although with a reduced gain, an advantage over the classical local bounds is preserved up to $\eta = 0.8$ (20% of losses), while the advantage is lost w.r.t. the classical capacity bound. It is worth noticing that the figure reported refers to gain per cell of information, so even a small fractions of information gained could result in a significant improvement over very large memories. In panel B the gain is reported as a function of the mean transmittance $\bar{\tau}_0$. Beside the overall reduction of the gain, in presence of losses we observe a widening of the low-informative region in the $\bar{\tau}_0$ range. Finally, in Figure 5 we compare the performance of the retrieval strategy proposed in this article with the one using only the two mean values of transmittance $\bar{\tau}_0$ and $\bar{\tau}_1$, ignoring the distributions characterizing the memory. The information $\mathcal{C}^{PC}$ recovered using classical states and photon counting is compared with the information $\mathcal{C}^{MV}$ recovered with the same resources but using only the mean values of the distributions. As expected, the characterization of the memory, i.e., the knowledge of the distribution of the physical parameter used for the encoding, and its use in the decision algorithm brings an advantage in the readout.

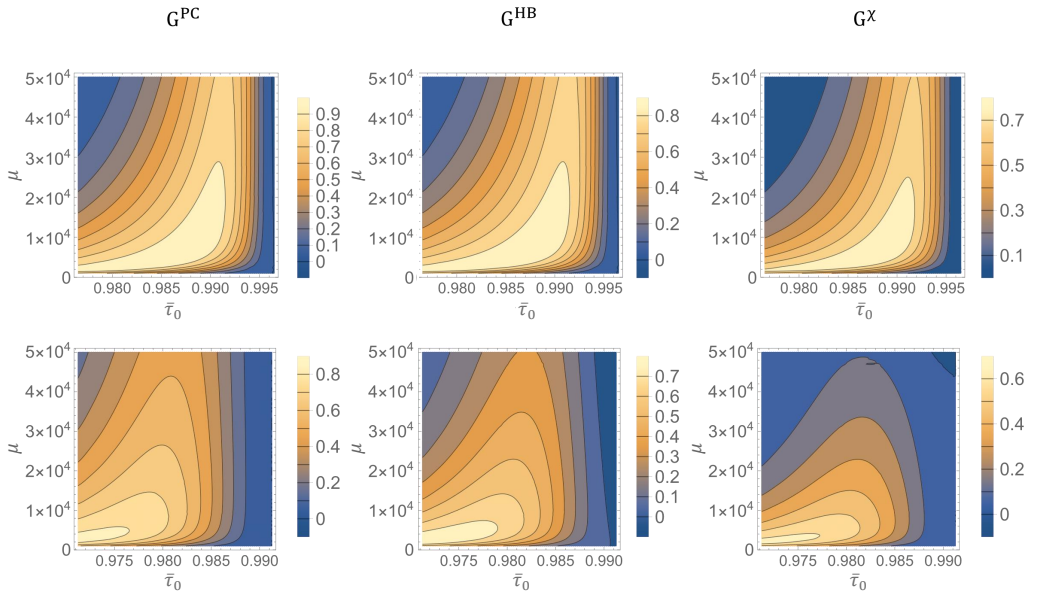

Figure 3. Quantum Gain. We show the quantum gain G as a function of the mean number of signal photons μ and the mean value of the transmittance $\bar{\tau}_0$ of one encoding distributions. In the upper row, the other parameters are fixed to $\sigma_0 = \sigma_1 = 0.001$ and $\bar{\tau}_1 = 0.997$. Starting from the left: G^{PC} is the quantum gain over to the performance of classical states an photon counting receiver, G^{HB} over the optimal bound of classical states considering local readout, and G^{χ} over the bound on the classical performance with global measurements. On the lower row we report the same figures of merit changing the parameters to $\sigma_0 = \sigma_1 = 0.0025$ and $\bar{\tau}_1 = 0.991$.

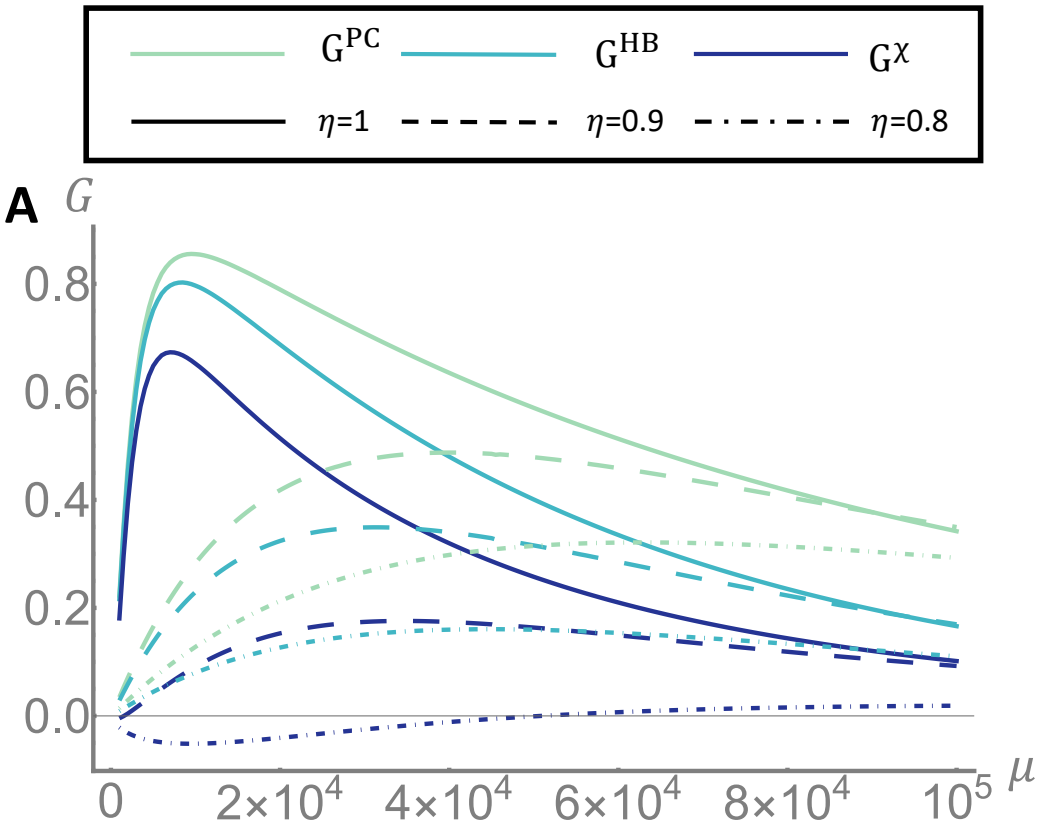

Figure 4. *Cont.*

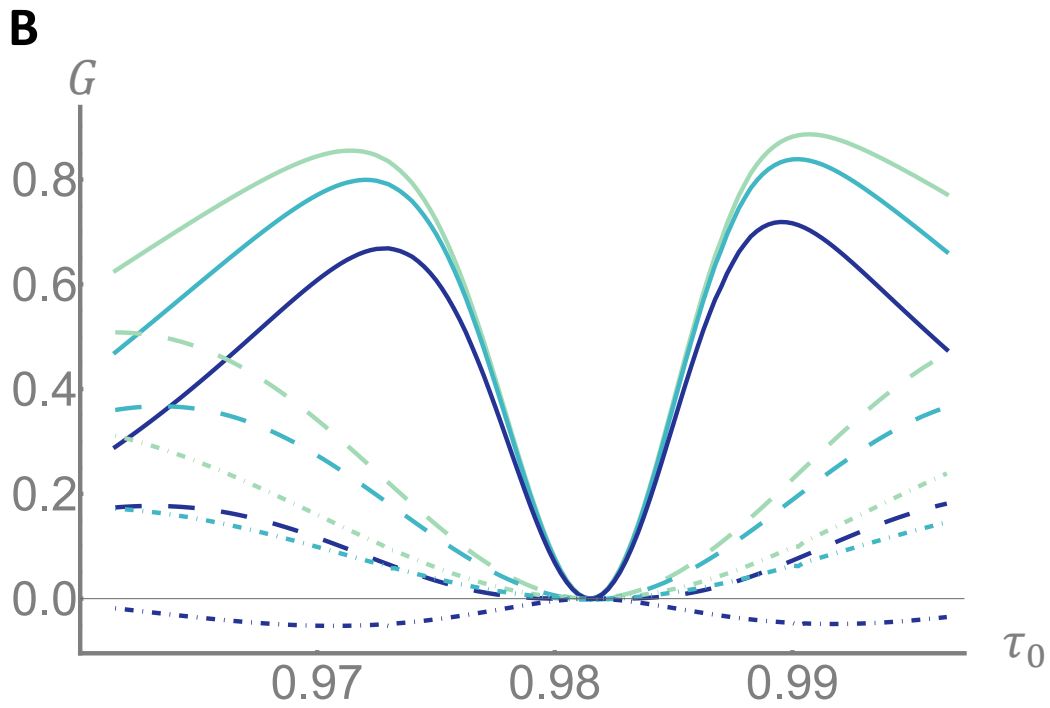

Figure 4. Inefficiency effect. We report the quantum gain over the three classical limit defined in the main text, for different values of overall efficiency η. In panel (**A**), we show the dependency of the gain on the main number of signal photons μ. The case of perfect efficiency $\eta = 1$ is reported in solid line, while the cases $\eta = 0.9$ an $\eta = 0.8$ are reported in dashed and dot dashed lines respectively. The distributions g_0 and g_1 are the same reported in the first row of Figure 2, namely $\bar{\tau}_0 = 0.972$, $\bar{\tau}_1 = 0.982$ and $\sigma_0 = \sigma_1 = 0.001$. In panel (**B**), we fix the number of photons to $\mu = 10^4$ and we show the dependency on the mean transmittance $\bar{\tau}_0$.

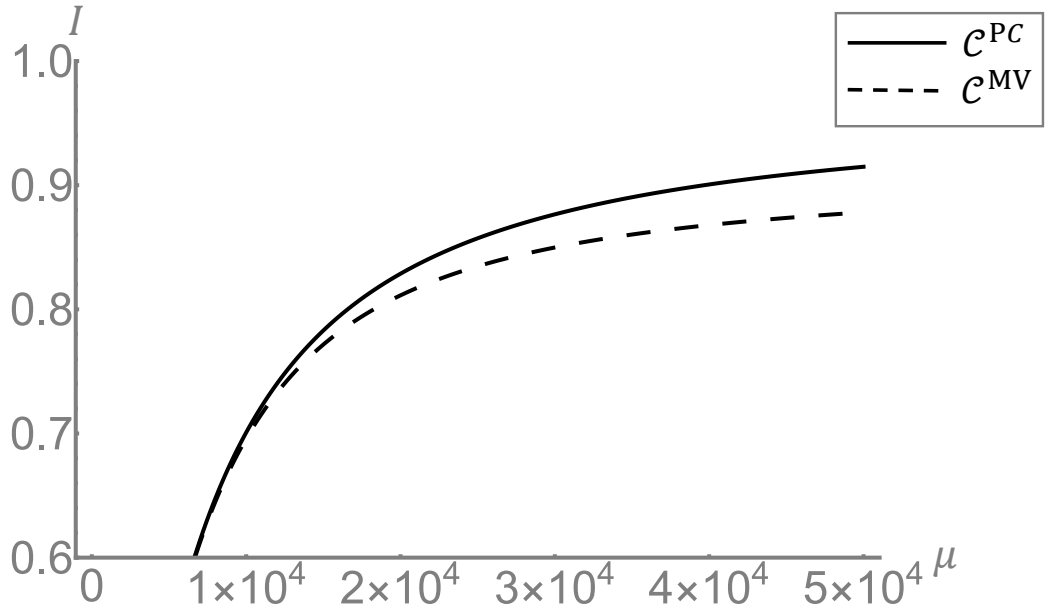

Figure 5. Post-processing comparison. We show the information retrieved by a classical transmitter and photon counting as a function of the mean number of signa photons μ. We consider two maximum likelihood post processing, one $\mathcal{C}^{PC}$, with full information on the distributions of T_0, and T_1, as discussed in the main text, and the other $\mathcal{C}^{MV}$ using only the mean values of the distributions $\bar{\tau}_0$ and $\bar{\tau}_1$. The parameters are fixed to $\bar{\tau}_0 = 0.925$, $\sigma_0 = 0.005$, $\bar{\tau}_1 = 0.965$ and $\sigma_1 = 0.01$.

4. Discussion

In this work we studied the effect of an imperfect characterization of a memory cell on its readout performance. In particular, we considered an optical memory storing a bit of information in two values of transmittance T_0 and T_1 that are not known with arbitrary precision, i.e., they are classical random variable with Gaussian distribution. In this scenario, we compared a specific quantum readout strategy, consisting of TMSV states transmitter and a photon counting receiver after the cell, with three classical informational limits: The classical optimal bound for a single cell readout, the classical performance achievable with a photon counting receiver and the classical capacity limit taking into account collective measurement on a large memory. Remarkably, the local quantum strategy reaches a notable advantage in terms of bit recovered per cell over all of them, even the last, global, one. Moreover, the advantage is retained for optical losses around 20%, which is particularly noticeable towards possible real applications, since losses represent the main limiting factor in many optical quantum sensing protocols. Finally, we have shown that taking properly into account the parameter distributions in the decision algorithm, when available, allows to optimize in general the readout performance. While this work is mainly focused on a model of digital memory the results can be applied to different scenario involving convex superposition of loss channels. Some example are the conformance test in the context of process monitoring, spectroscopy [48] and more in general any discrimination problem based on transmission/reflection optical measurement.

Author Contributions: Conceptualization, G.O and I.R.-B.; formal analysis, G.O.; methodology, G.O.; software, G.O; writing—original draft preparation, G.O.; writing—review and editing, G.O. and I.R.-B.; visualization, G.O. and I.R.-B.; supervision, I.R.-B.; funding acquisition, I.R.-B. All authors have read and agreed to the published version of the manuscript.

Funding: This work has been funded from the European Union's Horizon 2020 Research and Innovation Action under Grant Agreement No. 862644 (Quantum readout techniques and technologies, QUARTET).

Data Availability Statement: All data needed to evaluate the conclusions is reported in the paper.

Conflicts of Interest: The authors declare no conflict of interest.

Appendix A. Classical Capacity

As stated in the main text the imperfect memory readout problem can be seen as a problem of quantum channel discrimination. Given an input state ρ, for the retrieval one has to discriminate between the two channels acting on ρ as:

$$\begin{aligned}\rho_0 &= \mathbb{E}_{g_0}[(\mathcal{E}_\tau \otimes \mathcal{I})\rho] \\ \rho_1 &= \mathbb{E}_{g_1}[(\mathcal{E}_\tau \otimes \mathcal{I})\rho]\end{aligned} \tag{A1}$$

From an informational standpoint, a D cell memory encoding/readout can be seen as a transfer of information with each cell encoding the binary r.v. X in the ensemble $\{p_i, \rho_i\}$, $i = 0, 1$. For parallel probing of the memory some global encoding strategy could be more convenient than the direct one, encoding one bit per cell independently. One can consider an information retrieval strategy consisting of simultaneous probing of the whole memory and a joint global POVM measurement at the output (see Figure 1B in the main text). For a general encoding, if the input states are limited to tensor product states of the form $\rho^{\otimes D}$, the information per cell retrieved, I^D, can be upper bounded by the Holevo quantity χ:

$$I^D \leq \chi(\rho) := S(\rho_s) - \sum_i p_i S(\rho_i) \tag{A2}$$

where $\rho_s = \sum_i p_i \rho_i$ and $S(\rho) = -Tr(\rho \log \rho)$ is the von-Neumann entropy [47]. The less or equal sign in equation reflects the fact that for finite array of lenght D the convergence is not guaranteed. On the other hand for an infinite number of cells the the HWS theorem

guarantees the convergence of the information recovered by the optimal strategy to the Holevo quantity [47]. The information recovered depends on the input state ρ. As already done in the main text we will impose a constraint on the input states allowed in the form of a fixed signal number of photons μ. The optimization of the quantity would give an ultimate limit on the rate of information per bit that can be stored and retrieved accurately. However this optimization is not easy to perform on the full space of states. The problem can be solved more easily if the optimization is restricted to the class of classical states defined in Equation (2). Solving this optimization will yield the *classical capacity* of the imperfect memory, χ^{cla}:

$$\chi^{cla} := \max_{\rho_{cla}} \chi(\rho_{cla}) \tag{A3}$$

To find χ^{cla} we will first find the Holevo quantity for a single mode coherent state and then, following a similar proof given in Ref. [31] for a perfect memory, we will show how the quantity found is equal to the classical capacity.

Appendix A.1. Single Mode Coherent State

Consider a single mode coherent state $|\alpha\rangle\langle\alpha|$, without idler modes, as an input for the readout procedure. In this case the constraint on the number of photons gives the condition $|\alpha|^2 = \mu$. To compute the Holevo quantity for this state, χ^{α}, we first use the fact that pure loss channels map coherent states into coherent states, $\mathcal{E}_\tau(|\alpha\rangle\langle\alpha|) = |\sqrt{\tau}\alpha\rangle\langle\sqrt{\tau}\alpha|$, to compute the output states in Equation (A1):

$$\begin{aligned}\rho_0^{\alpha} &= \mathbb{E}_{g_0}[|\sqrt{\tau}\alpha\rangle\langle\sqrt{\tau}\alpha|] = \int d\tau g_0(\tau)|\sqrt{\tau}\alpha\rangle\langle\sqrt{\tau}\alpha| \\ \rho_1^{\alpha} &= \mathbb{E}_{g_1}[|\sqrt{\tau}\alpha\rangle\langle\sqrt{\tau}\alpha|] = \int d\tau g_1(\tau)|\sqrt{\tau}\alpha\rangle\langle\sqrt{\tau}\alpha|\end{aligned} \tag{A4}$$

where, since there are no idler modes, we omitted them from the notation. We have then:

$$\chi^{\alpha} = S(p_0\rho_0^{\alpha} + p_1\rho_1^{\alpha}) - \sum_i p_i S(\rho_i^{\alpha}) \tag{A5}$$

The computation of the entropy is complicated by the fact that the distribution g_i are in general continuous ones. To overcome this problem, we performed a uniform discretization of the distribution to some appropriate dimension K, so that the integrals over τ in Equation (A4) are substituted by finite sums, $\int d\tau \to \sum_i^k$. Under this approximation is easy to see how each entropy term in Equation (A5) can be rewritten as some convex combination of a finite subset of maximum dimension $2k$ of coherent states. The calculation of χ^{α} than can be reduced to the calculations of terms in the form:

$$S\left(\sum_{i=1}^{K} q_i|\sqrt{\tau_i}\alpha\rangle\langle\sqrt{\tau_i}\alpha|\right) \tag{A6}$$

where q_i are suitable probability coefficients depending on the initial distributions g_i and the term considered. For the first term on the right hand side of Equation (A5) the coefficients q_i will depend also on the ensemble probabilities p_i and the sum will in general be on $K = 2k$ terms. For the two entropy contributions on the summation the sum will go over $K = k$ terms.

In general, the set $\{|\sqrt{\tau_i}\alpha\rangle\}$ is a non-orthogonal basis of a K-dimensional Hilbert space. For any state $\rho = \sum_{i=1}^{K} q_i|\sqrt{\tau_i}\alpha\rangle\langle\sqrt{\tau_i}\alpha|$, we have:

$$S(\rho) = S(QG) \tag{A7}$$

where $Q = \mathrm{Diag}[q_i]$ and $G(i,j) = G(j,i) = \langle\sqrt{\tau_i}\alpha|\sqrt{\tau_j}\alpha\rangle$ are the elements of the Gram matrix G. In fact, we can write [49]:

$$S(\rho) = -\frac{\partial}{\partial n}\mathrm{Tr}(\rho^n)\Big|_{n=1} \tag{A8}$$

And

$$\begin{aligned}\mathrm{Tr}(\rho^n) &= \sum_{i_1,\ldots,i_n=1}^{K} q_{i_1}\cdots q_{i_n}\langle\sqrt{\tau_{i_1}}\alpha|\sqrt{\tau_{i_1}}\alpha\rangle\cdots\langle\sqrt{\tau_{i_n}}\alpha|\sqrt{\tau_{i_1}}\alpha\rangle = \\ &= \sum_{i_2,\ldots,i_n=1}^{K} q_{i_2}\cdots q_{i_n}\langle\sqrt{\tau_{i_2}}\alpha|\sqrt{\tau_{i_3}}\alpha\rangle\cdots\langle\sqrt{\tau_{i_{n-1}}}\alpha|\sqrt{\tau_{i_n}}\alpha\rangle GQG(i_n,i_2) = \\ &= \sum_{i_n=1}^{K} q_{i_n}G(QG)^{n-1}(i_n,i_n) = \mathrm{Tr}[(QG)^n]\end{aligned} \tag{A9}$$

Combining the results of Equations (A8) and (A9), we get the equality in Equation (A7).

While a closed form may not be available for a generic probability distribution and for arbitrary k, Equation (A7) allows to skip the orthogonalization of the subspace, which would represent a computational heavy task for large values of k. A numerical evaluation of χ^{α} can be performed using Equations (A7) and (A8). The Holevo quantity χ^{α} for the continuous set can be recovered as the limit for $k \to \infty$ of $\chi^{cla}(k)$. In the following section we will show how χ^{α} coincides with the classical capacity χ^{cla}.

Appendix A.2. Saturation of Capacity by Single Mode Coherent State

To prove that the classical capacity can be computed using a single mode coherent transmitter we can use the argument used in Ref. [31] that we report in the following.

Consider the class $\mathcal{P}$ of pure coherent transmitters. The class of mixed states formed by positive superposition of elements of $\mathcal{P}$ constitutes the class of classical states. Using the convexity on ρ of the Holevo information χ, it can be proved, similarly to what was done in [31], that, if the capacity of the class $\mathcal{P}$, χ^{P}, is concave in the number of photons μ, it must be larger or equal to the capacity of whole class of classical states:

$$\chi^{P} \geq \chi^{cla} \tag{A10}$$

Given that $\mathcal{P}$ belongs is a subclass of the classical states, the capacity of $\mathcal{P}$ cannot be larger than the one of classical states, so that Equation (A10) is an equality. The capacity of classical states is then saturated by pure coherent states. The concavity of $\chi_{\mathcal{P}}$ can be checked numerically.

To complete the proof, one must simply show that a single coherent mode saturates the capacity of $\mathcal{P}$. This can be done [31] using the fact that acting with unitary transformations, that don't change the von Neumann entropy, on the output states of any pure classical input one can rearrange the signal photons in a single mode obtaining the same result as a single mode input.

References

1. Giovannetti, V.; Lloyd, S.; Maccone, L. Advances in quantum metrology. *Nat. Photonics* **2011**, *5*, 222–229. [CrossRef]
2. Pirandola, S.; Bardhan, B.R.; Gehring, T.; Weedbrook, C.; Lloyd, S. Advances in photonic quantum sensing. *Nat. Photonics* **2018**, *12*, 724–733. [CrossRef]
3. Berchera, I.R.; Degiovanni, I.P. Quantum imaging with sub-Poissonian light: Challenges and perspectives in optical metrology. *Metrologia* **2019**, *56*, 024001. [CrossRef]
4. Giovannetti, V.; Lloyd, S.; Maccone, L. Quantum-Enhanced Measurements: Beating the Standard Quantum Limit. *Science* **2004**, *306*, 1330–1336. [CrossRef]
5. Schnabel, R. Squeezed states of light and their applications in laser interferometers. *Phys. Rep.* **2017**, *684*, 1–51. [CrossRef]
6. Schäfermeier, C.; Ježek, M.; Madsen, L.S.; Gehring, T.; Andersen, U.L. Deterministic phase measurements exhibiting super-sensitivity and super-resolution. *Optica* **2018**, *5*, 60–64. [CrossRef]
7. Ortolano, G.; Ruo-Berchera, I.; Predazzi, E. Quantum enhanced imaging of nonuniform refractive profiles. *Int. J. Quantum Inf.* **2019**, *17*, 1941010. [CrossRef]
8. Monras, A.; Paris, M.G.A. Optimal Quantum Estimation of Loss in Bosonic Channels. *Phys. Rev. Lett.* **2007**, *98*, 160401. [CrossRef]

9. Adesso, G.; Dell'Anno, F.; De Siena, S.; Illuminati, F.; Souza, L.A.M. Optimal estimation of losses at the ultimate quantum limit with non-Gaussian states. *Phys. Rev. A* **2009**, *79*, 040305. [CrossRef]
10. Losero, E.; Ruo-Berchera, I.; Meda, A.; Avella, A.; Genovese, M. Unbiased estimation of an optical loss at the ultimate quantum limit with twin-beams. *Sci. Rep.* **2018**, *8*, 7431. [CrossRef]
11. Brida, G.; Genovese, M.; Ruo Berchera, I. Experimental realization of sub-shot-noise quantum imaging. *Nat. Photonics* **2010**, *4*, 227–230. [CrossRef]
12. Genovese, M. Real applications of quantum imaging. *J. Opt.* **2016**, *18*, 073002. [CrossRef]
13. Aasi, J.; Abadie, J.; Abbott, B.P.; Abbott, R.; Abbott, T.D.; Abernathy, M.R.; Adams, C.; Adams, T.; Addesso, P.; Adhikari, R.X.; et al. Enhanced sensitivity of the LIGO gravitational wave detector by using squeezed states of light. *Nat. Photonics* **2013**, *7*, 613–619. [CrossRef]
14. Ruo Berchera, I.; Degiovanni, I.P.; Olivares, S.; Genovese, M. Quantum Light in Coupled Interferometers for Quantum Gravity Tests. *Phys. Rev. Lett.* **2013**, *110*, 213601. [CrossRef]
15. Pradyumna, S.T.; Losero, E.; Ruo-Berchera, I.; Traina, P.; Zucco, M.; Jacobsen, C.S.; Andersen, U.L.; Degiovanni, I.P.; Genovese, M.; Gehring, T. Twin beam quantum-enhanced correlated interferometry for testing fundamental physics. *Commun. Phys.* **2020**, *3*, 104. [CrossRef]
16. Helstrom, C. *Quantum Detection and Estimation Theory*; Academic Press: New York, NY, USA, 1976.
17. Chefles, A.; Barnett, S.M. Quantum state separation, unambiguous discrimination and exact cloning. *J. Phys. A* **1998**, *31*, 10097–10103. [CrossRef]
18. Lloyd, S. Enhanced Sensitivity of Photodetection via Quantum Illumination. *Science* **2008**, *321*, 1463–1465. [CrossRef]
19. Tan, S.H.; Erkmen, B.I.; Giovannetti, V.; Guha, S.; Lloyd, S.; Maccone, L.; Pirandola, S.; Shapiro, J.H. Quantum Illumination with Gaussian States. *Phys. Rev. Lett.* **2008**, *101*, 253601. [CrossRef]
20. Lopaeva, E.D.; Ruo Berchera, I.; Degiovanni, I.P.; Olivares, S.; Brida, G.; Genovese, M. Experimental Realization of Quantum Illumination. *Phys. Rev. Lett.* **2013**, *110*, 153603. [CrossRef]
21. Zhang, Y.; England, D.; Nomerotski, A.; Svihra, P.; Ferrante, S.; Hockett, P.; Sussman, B. Multidimensional quantum-enhanced target detection via spectrotemporal-correlation measurements. *Phys. Rev. A* **2020**, *101*, 053808. [CrossRef]
22. Gregory, T.; Moreau, P.A.; Toninelli, E.; Padgett, M.J. Imaging through noise with quantum illumination. *Sci. Adv.* **2020**, *6*, eaay2652. [CrossRef] [PubMed]
23. Pirandola, S. Quantum Reading of a Classical Digital Memory. *Phys. Rev. Lett.* **2011**, *106*, 090504. [CrossRef] [PubMed]
24. Nair, R. Discriminating quantum-optical beam-splitter channels with number-diagonal signal states: Applications to quantum reading and target detection. *Phys. Rev. A* **2011**, *84*, 032312. [CrossRef]
25. Wilde, M.M.; Guha, S.; Tan, S.; Lloyd, S. Explicit capacity-achieving receivers for optical communication and quantum reading. In Proceedings of the 2012 IEEE International Symposium on Information Theory Proceedings, Cambridge, MA, USA, 1–6 July 2012; pp. 551–555.
26. Dall'arno, M.; Bisio, A.; Mauro D'ariano, G. Ideal quantum reading of optical memories. *Int. J. Quantum Inf.* **2012**, *10*, 1241010. [CrossRef]
27. Dall'Arno, M.; Bisio, A.; D'Ariano, G.M.; Miková, M.; Ježek, M.; Dušek, M. Experimental implementation of unambiguous quantum reading. *Phys. Rev. A* **2012**, *85*, 012308. [CrossRef]
28. Hirota, O. Error Free Quantum Reading by Quasi Bell State of Entangled Coherent States. *Quantum Meas. Quantum Metrol.* **2017**, *4*, 70–73. [CrossRef]
29. Fernandes Pereira, F.R.; Mancini, S. Error Probability Mitigation in Quantum Reading Using Classical Codes. *Entropy* **2022**, *24*, 5. [CrossRef]
30. Ortolano, G.; Losero, E.; Pirandola, S.; Genovese, M.; Ruo-Berchera, I. Experimental quantum reading with photon counting. *Sci. Adv.* **2021**, *7*, eabc7796. [CrossRef]
31. Pirandola, S.; Lupo, C.; Giovannetti, V.; Mancini, S.; Braunstein, S.L. Quantum reading capacity. *New J. Phys.* **2011**, *13*, 113012. [CrossRef]
32. Zhuang, Q.; Pirandola, S. Entanglement-enhanced testing of multiple quantum hypotheses. *Commun. Phys.* **2020**, *3*, 103. [CrossRef]
33. Oskouei, S.K.; Mancini, S. Classical capacities of memoryless but not identical quantum channels. *Rev. Math. Phys.* **2021**, *33*, 2150012. [CrossRef]
34. Revson, F.; Mancini, S. Polar Codes for Quantum Reading. In Proceedings of the 2021 IEEE International Symposium on Information Theory (ISIT), Melbourne, Australia, 12–20 July 2021; pp. 2238–2243. [CrossRef]
35. Ortolano, G.; Boucher, P.; Degiovanni, I.P.; Losero, E.; Genovese, M.; Ruo-Berchera, I. Quantum conformance test. *Sci. Adv.* **2021**, *7*, eabm3093. [CrossRef] [PubMed]
36. Holevo, A.S. Bounds for the Quantity of Information Transmitted by a Quantum Communication Channel. *Probl. Inform. Transm.* **1973**, *9*, 177–183.
37. Holevo, A. The capacity of the quantum channel with general signal states. *IEEE Trans. Inf. Theory* **1998**, *44*, 269–273. [CrossRef]
38. Hausladen, P.; Jozsa, R.; Schumacher, B.; Westmoreland, M.; Wootters, W.K. Classical information capacity of a quantum channel. *Phys. Rev. A* **1996**, *54*, 1869–1876. [CrossRef] [PubMed]

39. Pirandola, S.; Laurenza, R.; Lupo, C.; Pereira, J.L. Fundamental limits to quantum channel discrimination. *NPJ Quantum Inf.* **2019**, *5*, 50. [CrossRef]
40. Zhuang, Q.; Pirandola, S. Ultimate Limits for Multiple Quantum Channel Discrimination. *Phys. Rev. Lett.* **2020**, *125*, 080505. [CrossRef]
41. Holevo, A.S. *Quantum Systems, Channels, Information: A Mathematical Introduction*; De Gruyter: Berlin, Germany, 2012. [CrossRef]
42. Braunstein, S.L.; van Loock, P. Quantum information with continuous variables. *Rev. Mod. Phys.* **2005**, *77*, 513–577. [CrossRef]
43. Weedbrook, C.; Pirandola, S.; García-Patrón, R.; Cerf, N.J.; Ralph, T.C.; Shapiro, J.H.; Lloyd, S. Gaussian quantum information. *Rev. Mod. Phys.* **2012**, *84*, 621–669. [CrossRef]
44. Bondani, M.; Allevi, A.; Zambra, G.; Paris, M.G.A.; Andreoni, A. Sub-shot-noise photon-number correlation in a mesoscopic twin beam of light. *Phys. Rev. A* **2007**, *76*, 013833. [CrossRef]
45. Avella, A.; Ruo-Berchera, I.; Degiovanni, I.P.; Brida, G.; Genovese, M. Absolute calibration of an EMCCD camera by quantum correlation, linking photon counting to the analog regime. *Opt. Lett.* **2016**, *41*, 1841–1844. [CrossRef] [PubMed]
46. Meda, A.; Losero, E.; Samantaray, N.; Scafirimuto, F.; Pradyumna, S.; Avella, A.; Ruo-Berchera, I.; Genovese, M. Photon-number correlation for quantum enhanced imaging and sensing. *J. Opt.* **2017**, *19*, 094002. [CrossRef]
47. Nielsen, M.A.; Chuang, I.L. *Quantum Computation and Quantum Information*, 10th ed.; Cambridge University Press: New York, NY, USA, 2011.
48. Shi, H.; Zhang, Z.; Pirandola, S.; Zhuang, Q. Entanglement-assisted absorption spectroscopy. *Phys. Rev. Lett.* **2020**, *125*, 180502. [CrossRef] [PubMed]
49. Gagatsos, C.N.; Karanikas, A.I.; Kordas, G.; Cerf, N.J. Entropy generation in Gaussian quantum transformations: Applying the replica method to continuous-variable quantum information theory. *npj Quantum Inf.* **2016**, *2*, 15008. [CrossRef]